Anomalous Edge Transport in the Quantum Anomalous Hall State

Jing Wang, Biao Lian, Haijun Zhang, and Shou-Cheng Zhang

Department of Physics, McCullough Building, Stanford University, Stanford, California 94305-4045, USA

(Received 7 June 2013; published 20 August 2013)

We predict by first-principles calculations that thin films of a Cr-doped $(Bi, Sb)_2Te_3$ magnetic topological insulator have gapless nonchiral edge states coexisting with the chiral edge state. Such gapless nonchiral states are not immune to backscattering, which would explain dissipative transport in the quantum anomalous Hall (QAH) state observed in this system experimentally. Here, we study the edge transport with both chiral and nonchiral states by the Landauer-Büttiker formalism and find that the longitudinal resistance is nonzero, whereas Hall resistance is quantized to h/e^2. In particular, the longitudinal resistance can be greatly reduced by adding an extra floating probe even if it is not used, while the Hall resistance remains at the quantized value. We propose several transport experiments to detect the dissipative nonchiral edge channels. These results will facilitate the realization of pure dissipationless transport of QAH states in magnetic topological insulators.

DOI: 10.1103/PhysRevLett.111.086803 PACS numbers: 73.20.−r, 73.40.−c, 73.43.Qt, 73.23.−b

Introduction.—The recent theoretical prediction and experimental realization [1–6] of the quantum anomalous Hall (QAH) effect have generated intense interest in this new state of quantum matter. The QAH insulator has a topologically nontrivial electronic structure characterized by a bulk energy gap but gapless chiral edge states, leading to the quantized Hall effect without an external magnetic field [7]. In the quantum Hall effect (QHE), electronic states of a two-dimensional (2D) electron system form Landau levels under a strong external magnetic field, and the Hall resistance is accurately quantized into $h/\nu e^2$ plateaus [8,9] accompanied by exact zero longitudinal resistance and conductance in the plateaus (here, h is Plank's constant, e is the charge of an electron, and ν is an integer or a certain fraction). The exact quantization of the Hall resistance arises from dissipationless chiral states localized at sample edges [10], along which electric currents flow unidirectionally and backscattering cannot take place [11]. In a QAH insulator, theoretically predicted in magnetic topological insulators (TIs) [1–5], the spin-orbit coupling (SOC) and ferromagnetic ordering combine to give rise to a topologically nontrivial phase characterized by a finite Chern number [12] and chiral edge states characteristic of the QAH state. The QAH effect has been experimentally observed in thin films of Cr-doped $(Bi, Sb)_2Te_3$ magnetic TIs [6], where at zero magnetic field, the gate-tuned Hall resistance (ρ_{xy}) exhibits a plateau with quantized value h/e^2 while the longitudinal resistance (ρ_{xx}) shows a dip down to $0.098h/e^2$. This quantized value of ρ_{xy} is consistent with quantum transport due to a single chiral edge state. However, nonzero ρ_{xx} indicates that the system has other dissipative conduction channels. Thus, it is important to be able to trace where such dissipation comes from and to realize experimentally a pure dissipationless transport of QAH states in magnetic TIs [13].

In this Letter, based on first-principles calculations, we show that five quintuple layers (QLs) of $Cr_x(Bi, Sb)_{2-x}Te_3$ studied in the experiment [6] have gapless nonchiral edge states coexisting with a chiral edge state. Such gapless nonchiral states are not immune to backscattering, which would explain dissipative transport of the recent QAH experiment [6]. Here, we study the edge transport with both chiral and nonchiral states by the Landauer-Büttiker formula and find that ρ_{xx} exhibits non-Ohmic behavior. Remarkably, ρ_{xx} is nonzero, whereas ρ_{xy} is quantized into h/e^2. In particular, ρ_{xx} can be greatly reduced by the mere presence of a floating probe even if it is not used, while ρ_{xy} remains at the quantized value. The nonchiral edge channels can be detected through nonlocal transport measurements. We also predict that thinner films of Cr-doped $(Bi, Sb)_2Te_3$ are a QAH insulator with a single chiral edge state, in which pure dissipationless transport of QAH states can be realized.

Materials.—We study the Cr-doped $(Bi_{0.1}Sb_{0.9})_2Te_3$ magnetic TI, where the Dirac cone of the surface states is observed to be located in the bulk band gap [6,14]. Here, we carry out first-principles calculations on three-dimensional $(Bi_{0.1}Sb_{0.9})_2Te_3$ without SOC, where the virtual crystal approximation is employed to simulate the mixing between Bi and Sb. Then, we construct the tight-binding model with SOC and the exchange interaction based on maximally localized Wannier functions [15,16]. The effective SOC parameter of $Cr_x(Bi_{0.1}Sb_{0.9})_{2-x}$ is obtained by linear interpolation between the SOC strength of Bi and Sb, where the reduced SOC strength resulting from the Cr substitution of (Bi, Sb) has been taken into account [17]. When the 2D system stays in the QAH phase, there must be chiral edge states if an edge is created. Here, we study the edge states of $Cr_x(Bi, Sb)_{2-x}Te_3$ thin films along the *edge A* direction, as shown in Fig. 1. For a semi-infinite system, combining the tight-binding model with

 © 2013 American Physical Society

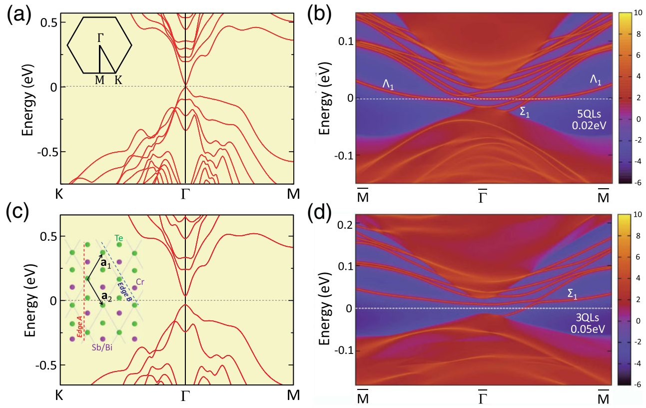

FIG. 1 (color online). Band structures for five QLs and three QLs $Cr_{0.15}(Bi_{0.1}Sb_{0.9})_{1.85}Te_3$ without an exchange field are plotted in (a) and (c), respectively. The dashed line indicates the Fermi level. The inset of (a) shows the 2D Brillouin zone with high-symmetry **k** points $\Gamma(0,0)$, $K(\pi,\pi)$, and $M(\pi,0)$ labeled, and that of (c) is the top view of a 2D thin film with two in-plane lattice vectors $\mathbf{a}_1$ and $\mathbf{a}_2$. The 1D edges are indicated by the dashed lines, *edge A* and *edge B*. The energy dispersion of a thin film along *edge A* is plotted for (b) five QLs with exchange field 0.02 eV and (d) three QLs with exchange field 0.05 eV. Here, the warmer colors (lighter gray in gray scale) represent the higher local density of states, with red (light gray) and blue (dark gray) regions indicating 2D bulk energy bands and energy gaps, respectively. The gapless edge states can be clearly seen around the Γ point as red (light gray) lines dispersing in the 2D bulk gap. One gapless chiral edge state Σ_1 and one pair of gapless quasihelical edge states Λ_1 coexist in (b), while only one gapless chiral edge state Σ_1 exists in (d).

the iterative method [18], we can calculate the Green's function for the edge states directly. The local density of states is related to the imaginary part of the Green's function, from which we obtain the dispersion of edge states (see the Supplemental Material [19]). As shown in Fig. 1(b) for five QLs $Cr_{0.15}(Bi_{0.1}Sb_{0.9})_{1.85}Te_3$, there indeed exists one chiral edge state Σ_1 indicating the $\nu = 1$ QAH state. There are also other trivial edge states, but most of them only connect to the conduction or valence bands. Remarkably, one pair of these trivial edge states Λ_1 is gapless, which connects the conduction and valence bands.

Λ_1 can be dubbed as the *quasihelical* edge states. It originates from helical edge states of the quantum spin Hall (QSH) effect but with time-reversal symmetry (TRS) breaking due to spontaneous magnetic moments, where the gap is opened at the Dirac point and buried into valence bands by particle-hole asymmetry. It is nonchiral, with two counterpropagating channels, but not immune to backscattering due to TRS breaking. Such coexistence of chiral and quasihelical edge states is quite general in magnetic TIs, especially in thick films. These quasihelical states do not change the topological property of the system; however, they contribute to the dissipative edge transport and can be used to explain nonzero ρ_{xx} when ρ_{xy} is quantized in the QAH experiment [6].

Edge transport.—To demonstrate the existence of predicted extended nonchiral edge channels in magnetic TIs, we study the edge transport with both chiral and nonchiral states by the Landauer-Büttiker formalism [20,21]. The general relationship between current and voltage is expressed as

$$I_i = \frac{e^2}{h}\sum_j (T_{ji}V_i - T_{ij}V_j), \tag{1}$$

where V_i is the voltage on the ith electrode, I_i is the current flowing out of the ith electrode into the sample, and T_{ji} is the transmission probability from the ith to the jth electrodes. There is no net current ($I_j = 0$) on a voltage lead or floating probe j, and the total current is conserved, namely, $\sum_i I_i = 0$. The current is zero when all the potentials are equal, implying the sum rules $\sum_i T_{ji} = \sum_i T_{ij}$.

For a standard Hall bar with $\mathcal{N}$ current and voltage leads [such as Fig. 2(a) with $\mathcal{N} = 6$], the transmission matrix elements for the chiral state of the $\nu = 1$ QAH effect are given by $T_{i+1,i} = 1$, for $i = 1, \ldots, \mathcal{N}$, and others $= 0$. (Here, we identify $i = \mathcal{N} + 1$ with $i = 1$.) For quasihelical states, $T_{i+1,i} = k_1$, $T_{i,i+1} = k_2$, and others $= 0$. These states are not protected from backscattering, and the transmission from one electrode to the next is not perfect, implying $k_1, k_2 < 1$, which is different from helical edge states in the QSH effect where $k_1 = k_2 = 1$ [22]. For simplicity, we have assumed T_{ij} to be translational invariant, namely, $T_{ij} = T_{i+1,j+1}$. In general, k_1 and k_2 become zero for an infinitely large sample because either dissipation occurs once the phase coherence is destroyed in the metallic leads or the momentum is relaxed when the sample size $L \gg$ the mean free path l_m [$k_1, k_2 \sim l_m/(l_m + L)$]. By contrast, the QAH chiral edge states are

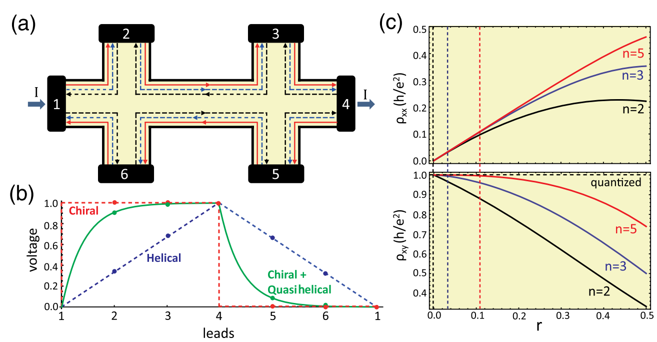

FIG. 2 (color online). Hall bridge and transport properties. (a) Schematic drawing of a Hall bar device with both quasihelical edge channels (dashed lines) and a chiral edge channel (solid lines). The current is from terminals 1 to 4; voltage leads are on electrodes 2, 3, 5, and 6. (b) Voltage at terminals 1–6 for transport of the chiral, helical, and chiral and quasihelical edge states. The transport with both chiral and quasihelical edge channels (solid lines) show non-Ohmic behaviors of ρ_{xx}. (c) ρ_{xx} and ρ_{xy} vs r with different numbers of effective voltage leads on each side of the sample.

robust against phase decoherence. Thus, the nonzero total transmission matrix elements are

$$T_{i+1,i} = 1 + k_1, \qquad T_{i,i+1} = k_2. \tag{2}$$

In the case of current leads on electrodes 1 and 4 and voltage leads on electrodes 2, 3, 5, and 6, as shown in Fig. 2(a), one finds that $I_1 = -I_4 \equiv I$, and the voltage from 1, 2, 3, to 4 increases exponentially, whereas the voltage from 4, 5, 6, to 1 decreases exponentially

$$V_j = \frac{1 - r^{j-1}}{1 - r^3} V, \qquad 1 \le j \le 4, \tag{3}$$

$$V_j = \frac{1 - r^{j-7}}{1 - r^{-3}} V, \qquad 4 \le j \le 6. \tag{4}$$

Here, we set $V_1 \equiv 0$ and $V_4 \equiv V$, and $r \equiv k_2/(1 + k_1)$. If $k_1 = k_2 = 0$, which is the case for chiral edge state transport in the QAH effect and QHE, $V_2 = V_3 = V = (h/e^2)I$ and $V_5 = V_6 = 0$, so that $\rho_{xy} \equiv (V_2 - V_6)/I = h/e^2$ and $\rho_{xx} \equiv (V_3 - V_2)/I = 0$ as expected [shown in Fig. 2(b)]. For the helical edge state transport in the QSH effect with $T_{i+1,i} = T_{i,i+1} = 1$, $V_2 = V_6 = V/3 = (h/2e^2)I$, and $V_3 = V_5 = 2V/3$, and thus $R_{14,14} \equiv (V_4 - V_1)/I = 3h/2e^2$ and $R_{14,23} \equiv (V_3 - V_2)/I = h/2e^2$ [22]. For the edge transport with both chiral and quasihelical states, the voltages of different leads are plotted in Fig. 2(b), where ρ_{xx} does not scale linearly with the spacing between the voltage leads in accordance with Ohm's law. Moreover, ρ_{xx} is nonzero, while ρ_{xy} is nearly quantized. This is the key result of this Letter. The sample size in experiment is $>200\ \mu$m, which is much larger than phase coherence length $l_\phi < 1\ \mu$m in this material with a rather low mobility ($< 800\ \text{cm}^2/\text{V s}$) [6,23]. The effect of decoherence between two real leads can be modeled as an extra floating lead, in which quasihelical states interact with infinitely many low-energy degrees of freedom, completely losing their phase coherence [22]. Thus, the standard Hall bar with $\mathcal{N} = 6$ current and voltage leads [shown in Fig. 2(a)] used in experiment has effectively $n = 5$ voltage leads on each side. As shown explicitly in Fig. 2(c), for a certain parameter range of r, ρ_{xy} can be quantized to a h/e^2 plateau, whereas ρ_{xx} is nonzero. This explains the dissipative longitudinal transport of the QAH effect observed in magnetic TIs recently [6].

In the presence of a strong external magnetic field B, the backscattering of quasihelical edge states is enhanced due to breaking of the TRS, while the chiral edge state is robust against backscattering. When the magnetic length $l_B < l_m$ ($l_B \sim \sqrt{\hbar/eB} \sim 10$ nm at 10 T), similar to the one-dimensional antilocalization, the enhanced backscattering makes both k_1 and k_2 approaching zero, and thus ρ_{xx} decreases as B increases [6]. In an even higher magnetic field, the transition to an ordinary quantum Hall state takes place. The quasihelical edge states disappear with $k_1 = k_2 = 0$; only the chiral state of the QHE survives; therefore, ρ_{xx} vanishes completely in a high magnetic field. This scenario is consistent with the experimental observations [6].

In reality, voltage leads may not be correctly aligned experimentally, as illustrated in Fig. 3(a), where the current leads are on electrodes 1 and 4. Suppose electrodes 2 and 6′ are voltage leads in experiment, while position 6 is the symmetric point (mirror) of 2. The voltage of leads in this Hall bar is plotted in Fig. 3(b). The solid line and dashed line denote the voltages of leads when magnetization **M** is up (↑) and down (↓), respectively. If the leads are symmetric,

$$\rho_{xy}(\Uparrow) = \frac{V_2^{\Uparrow} - V_6^{\Uparrow}}{I} = -\frac{V_2^{\Downarrow} - V_6^{\Downarrow}}{I} = -\rho_{xy}(\Downarrow) \equiv \rho_0.$$

If the leads are not symmetric, namely, 6 is moved to 6′, effectively, such misalignment of leads will cause $V_{6'}$ to be higher than V_6 independent of magnetization. So, the Hall resistance ρ'_{xy} measured between 2 and 6′ will gain a fraction of the longitudinal resistance

$$\rho'_{xy}(\Uparrow) = \rho_0 - \frac{V_{6'}^{\Uparrow} - V_6^{\Uparrow}}{I} = \rho_0 - \Delta\rho(\Uparrow), \tag{5}$$

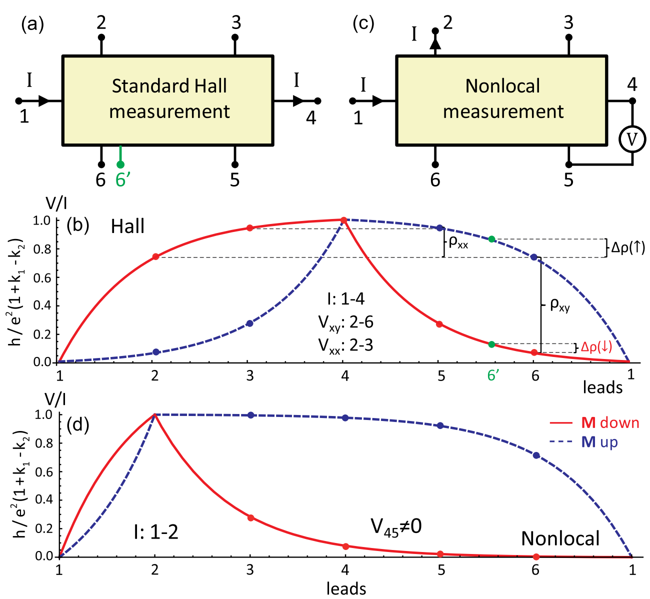

FIG. 3 (color online). Six-terminal Hall and nonlocal measurements. (a) Standard Hall measurement with six terminals and (b) corresponding voltages. The current is through 1 to 4, and the Hall voltage is measured between 2 and 6. Terminal 6 (denoted as 6′) is not be symmetric to terminal 2 due to misalignment, so the Hall signal may contain some longitudinal component. (c) Nonlocal measurement and (d) voltage. The current is through 1 to 2. In (b) and (d), the voltages with downward and upward magnetic orderings are denoted as solid red and dashed blue lines, respectively.

$$\rho'_{xy}(\downarrow) = -\rho_0 - \frac{V^{\downarrow}_{6'} - V^{\downarrow}_{6}}{I} = -\rho_0 - \Delta\rho(\downarrow). \quad (6)$$

Thus, $\rho'_{xy}(\uparrow) \neq -\rho'_{xy}(\downarrow)$. To the lowest order, $\Delta\rho(\uparrow) \approx \Delta\rho(\downarrow)$, and one can antisymmetrize the Hall resistance to eliminate the effect of asymmetric leads

$$\rho_{xy} = \frac{\rho'_{xy}(\uparrow) - \rho'_{xy}(\downarrow)}{2}. \quad (7)$$

For a well quantized ρ_{xy}, one of $\rho'_{xy}(\uparrow)$ and $\rho'_{xy}(\downarrow)$ will be larger than h/e^2, while the other will be smaller. This is exactly the phenomenon observed in the QAH experiment [6]. It is worth mentioning that in this system, $\Delta\rho(\uparrow) \neq \Delta\rho(\downarrow)$, so this antisymmetrization process does not cancel the asymmetry effect completely.

Nonlocal transport.—The dissipative transport measured in the standard Hall bar does not allow us to distinguish experimentally between quasihelical edge channels and residual bulk conduction channels in a convincing manner. An unambiguous way to prove the existence of quasihelical edge state transport in the QAH experiment is to use nonlocal electrical measurements. The edge states necessarily lead to nonlocal transport, and such nonlocal transport has been experimentally observed in the QHE [20,24], which provides definitive evidence for the existence of chiral edge states in the QHE.

As shown in Figs. 3(c) and 3(d), a current is passed through probes 1 and 2 and voltage is measured between probes 4 and 5 away from the dissipative bulk current path. For chiral edge state transport, the voltage signal tends to zero. However, for the transport of quasihelical edge states, $V_4 - V_5 \neq 0$, which gives a nonlocal resistance signal $R_{12,45}/\rho_{xx} \approx 0.1$ (around 220 Ω). Here, ρ_{xx} is the longitudinal resistance measured by current flowing through 1 to 4 and the voltage between 2 and 3. The classical Ohmic bulk contribution to the nonlocal (NL) effect is given by $\mathcal{R}^{\text{classical}}_{\text{NL}}/\rho_{xx} \approx \exp(-\pi\ell/w)$, where ℓ is the distance between the voltage probes and w is the strip width [25]. For the geometry with $\ell/w = 2$, we estimate $\mathcal{R}^{\text{classical}}_{\text{NL}}/\rho_{xx} \approx 10^{-3}$ (5 Ω). Therefore, one would only expect a minimal signal from a conducting bulk. Different from bulk conduction, the quasihelical edge states are fully nonlocal, and this signature can be taken as strong evidence for the existence of quasihelical edge channel transport in the QAH experiment. One can further measure the voltage between electrodes 3 and 4, and also that between 5 and 6. Quantitatively, for edge transport, $(V_3 - V_4)/(V_4 - V_5) = (V_4 - V_5)/(V_5 - V_6)$, which can further verify the extra dissipative edge channels in magnetic TIs. A similar nonlocal voltage can also be studied in a different geometry, for example, in the shape of the letter H, as shown in Fig. 4(c). The current leads on 1 and 4, and the voltage leads on 2 and 3.

Another transport measurement that could directly confirm the existence of quasihelical edge channels is shown

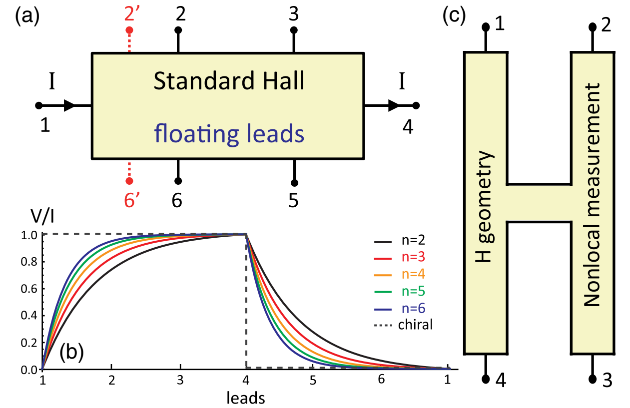

FIG. 4 (color online). Transport measurements with different numbers of terminals and device geometry. (a) Standard Hall measurement with extra floating terminals 2′ and 6′ inserted at the edges. I, 1–4; V_{xy}, 2–6; and V_{xx}, 2–3. (b) The voltage at terminals 1–6 of (a) in the presence of extra floating probes. n denotes the total numbers of voltage probes on one side. The dashed line denotes the chiral edge state transport, which is not affected by extra floating probes. (c) Nonlocal four-terminal resistance and two-terminal resistance measurements on the H-bar device.

in Fig. 4(a), where extra floating probes 2′ and 6′ are added to the standard Hall bar [26]. For the $\nu = 1$ QAH effect in magnetic TIs, such extra floating leads at sample edges will not affect the transport of residual bulk conduction channels, if there are any. It also will not affect the chiral edge channel transport. However, it will establish an equilibrium between the two counterpropagating channels of the quasihelical edge states and changes ρ_{xx} and ρ_{xy}. By adding more extra floating probes, ρ_{xx} approaches 0 and ρ_{xy} is more accurately quantized into h/e^2, as illustrated in Fig. 4(b). This is a rather sharp feature which is easy to implement in experiments.

Finally, we discuss the Corbino geometry [11] for the QAH effect. The theory proposed here would predict that the current flows from the inner to the outer rings of the Corbino disk would be zero, since there are no bulk carriers. The quasihelical edge states do not contribute to the currents in the Corbino disk. Therefore, the quantization of Hall resistance is exact.

In summary, the coexistence of chiral and quasihelical edge channels in magnetic TIs can explain the dissipative longitudinal transport of the recent QAH experiment. Such quasihelical edge states can be detected by nonlocal transport measurements. In fact, thinner films of magnetic TIs such as three QLs $Cr_{0.15}(Bi_{0.1}Sb_{0.9})_{1.85}Te_3$ are QAH insulators with a single chiral edge state as shown in Fig. 1(d). There is no gapless trivial edge state in this system, and one can realize the completely dissipationless transport of QAH states.

We acknowledge C. Z. Chang and Q. K. Xue for valuable discussions. This work is supported by the Defense

Advanced Research Projects Agency, Microsystems Technology Office, MesoDynamic Architecture Program (MESO), through Contract No. N66001-11-1-4105; the DARPA Program on "Topological Insulators—Solid State Chemistry, New Materials and Properties," under Grant No. N66001-12-1-4034; and by the U.S. Department of Energy, Office of Basic Energy Sciences, Division of Materials Sciences and Engineering, under Contract No. DE-AC02-76SF00515.

[1] X.-L. Qi, Y.-S. Wu, and S.-C. Zhang, Phys. Rev. B **74**, 085308 (2006).
[2] X.-L. Qi, T. L. Hughes, and S.-C. Zhang, Phys. Rev. B **78**, 195424 (2008).
[3] C.-X. Liu, X.-L. Qi, X. Dai, Z. Fang, and S.-C. Zhang, Phys. Rev. Lett. **101**, 146802 (2008).
[4] R. Li, J. Wang, X. L. Qi, and S. C. Zhang, Nat. Phys. **6**, 284 (2010).
[5] R. Yu, W. Zhang, H.-J. Zhang, S.-C. Zhang, X. Dai, and Z. Fang, Science **329**, 61 (2010).
[6] C.-Z. Chang, J. Zhang, X. Feng, J. Shen, Z. Zhang, M. Guo, K. Li, Y. Ou, P. Wei, L.-L. Wang, Z.-Q. Ji, Y. Feng, S. Ji, X. Chen, J. Jia, X. Dai, Z. Fang, S.-C. Zhang, K. He, Y. Wang, L. Lu, X.-C. Ma, and Q.-K. Xue, Science **340**, 167 (2013).
[7] F. D. M. Haldane, Phys. Rev. Lett. **61**, 2015 (1988).
[8] K. v. Klitzing, G. Dorda, and M. Pepper, Phys. Rev. Lett. **45**, 494 (1980).
[9] D. C. Tsui, H. L. Stormer, and A. C. Gossard, Phys. Rev. Lett. **48**, 1559 (1982).
[10] R. B. Laughlin, Phys. Rev. B **23**, 5632 (1981).
[11] B. I. Halperin, Phys. Rev. B **25**, 2185 (1982).
[12] D. J. Thouless, M. Kohmoto, M. P. Nightingale, and M. den Nijs, Phys. Rev. Lett. **49**, 405 (1982).
[13] J. Wang, B. Lian, H. Zhang, Y. Xu, and S.-C. Zhang, arXiv:1305.7500.
[14] J. Zhang, C.-Z. Chang, Z. Zhang, J. Wen, X. Feng, K. Li, M. Liu, K. He, L. Wang, X. Chen, Q.-K. Xue, X. Ma, and Y. Wang, Nat. Commun. **2**, 574 (2011).
[15] N. Marzari and D. Vanderbilt, Phys. Rev. B **56**, 12 847 (1997).
[16] I. Souza, N. Marzari, and D. Vanderbilt, Phys. Rev. B **65**, 035109 (2001).
[17] J. Zhang, C.-Z. Chang, P. Tang, Z. Zhang, X. Feng, K. Li, L.-l. Wang, X. Chen, C. Liu, W. Duan, K. He, Q.-K. Xue, X. Ma, and Y. Wang, Science **339**, 1582 (2013).
[18] M. P. L. Sancho, J. M. L. Sancho, and J. Rubio, J. Phys. F **14**, 1205 (1984).
[19] See Supplemental Material at http://link.aps.org/supplemental/10.1103/PhysRevLett.111.086803 for technical details of the first-principles calculations on the band structure and edge states.
[20] M. Büttiker, Phys. Rev. Lett. **57**, 1761 (1986).
[21] M. Büttiker, Phys. Rev. B **38**, 9375 (1988).
[22] A. Roth, C. Brne, H. Buhmann, L. W. Molenkamp, J. Maciejko, X.-L. Qi, and S.-C. Zhang, Science **325**, 294 (2009).
[23] M. Liu, C.-Z. Chang, Z. Zhang, Y. Zhang, W. Ruan, K. He, L.-l. Wang, X. Chen, J.-F. Jia, S.-C. Zhang, Q.-K. Xue, X. Ma, and Y. Wang, Phys. Rev. B **83**, 165440 (2011).
[24] C. W. J. Beenakker and H. van Houten, Solid State Phys. **44**, 1 (1991).
[25] L. J. van der Pauw, Philips Tech. Rev. **20**, 220 (1958), http://electron.mit.edu/~gsteele/vanderpauw/vanderpauw.pdf.
[26] S. Datta, *Electronic Transport in Mesoscopic Systems* (Cambridge University Press, Cambridge, England, 1995).